Chinese Chemical Letters 31 (2020) 119–124

Contents lists available at ScienceDirect

Chinese Chemical Letters

journal homepage: www.elsevier.com/locate/cclet

Communication

Synthesis of two A-B-C type conjugated amphiphilic triblock fullerene derivatives and their application in organic solar cells

Jikang Liu, Pengfei Jiang, Yao Wang, Guoli Tu*

Wuhan National Laboratory for Optoelectronics, Huazhong University of Science and Technology, Wuhan 430074, China

ARTICLE INFO

Article history:
Received 1 April 2019
Received in revised form 19 April 2019
Accepted 13 May 2019
Available online 13 May 2019

Keywords:
Amphiphilic triblock fullerene derivatives
Interfacial dipoles
Interface compatibility
Self-assembly
Water contact angle

ABSTRACT

Two A-B-C type conjugated amphiphilic triblock fullerene derivatives C_{60}-2HMTPB and C_{60}-2EHTPB were obtained in multi steps synthesis with three different blocks, and the amphiphilic diblock molecular C_{60}-4TPB was also preferred as a reference. When as modifying layer on zinc oxide (ZnO), the three fullerene derivatives can all reduce the work function of ZnO *via* modulation of the interfacial dipoles and lead a better electrical coupling. As introducing treatment of toluene, the obvious self-assembly of fullerene derivatives were observed, which were supported by X-ray diffraction and contact angle of water measurement. Base on PTB7-Th:$PC_{71}BM$ system, the inverted organic solar cells devices with structure of ITO/ZnO/fullerene derivatives/PTB7-Th:$PC_{71}BM$/MoO_3/Al got power conversion efficiencies of 8.62%, 8.83% and 9.00% for C_{60}-4TPB, C_{60}-2HMTPB and C_{60}-2EHTPB, respectively, compared 8.13% of devices with bare ZnO. The result of conjugated amphiphilic triblock fullerene derivatives provides a straightforward approaching by simultaneously modulating the morphology and interfacial work function of ZnO, which can also lead high performance in optoelectronic devices.

The simplest conjugated amphiphilic molecules have two well-defined blocks of hydrophilic head and hydrophobic tail, which can exhibit very promising properties based on microphase separation [1–5]. However, both the two blocks can influence each other's aggregation behavior, which might lead to an unfriendly behavior of the application of conjugated amphiphilic molecules [6,7]. The addition of a third block with physico-chemical properties different from the tail and head blocks, can be acted as the linker block to expand the possibilities for self-assembly of the conjugated amphiphilic triblock molecule [8–10]. Alternatively, the conjugated amphiphilic triblock molecule with three different blocks can also be named as A-B-C type molecule, can self-assemble in solution or with a solvent annealing [11–13].

With the advantage of offering a high transparency and atomically smooth surfaces, zinc oxide (ZnO) in particular has been widely used as an electron-selective material to modify the bottom cathode contact in organic solar cells (OSCs) with an inverted architecture [14–22]. However, the effectiveness of ZnO layer was found to be strongly dependent on their surface properties and on the trap sites and defects present there [23–29]. An effective approach to solve these problems is to modify the ZnO surface with a self-assembled monolayer of organic molecules such as fullerene derivatives [30–36]. So a great number of functional fullerene derivatives have been developed and incorporated as a modification layer on ZnO [37–40]. Fullerene derivative which functionalized with anchoring groups (such as sulfonate, ether chain, ester and carboxylic acid) have been successfully used as a modification layer to decrease defects of ZnO with interfacial dipole formed by hydrophilic group of fullerene derivatives [41–44]. The fullerene derivatives can be easily processed through a solution-based spin-coating method, which could also demonstrate a good compatibility between organic active layer and ZnO. The preparation of ZnO/fullerene derivatives also had no degradation of the underlying ZnO layer, which was due to the good solubility of fullerene derivative material in polarity solution [45,46].

In this work, two A-B-C type conjugated amphiphilic triblock molecular with different hydrophilic block named [6,6]-phenyl-C_{61}-butyricacid-2-(4-(9,9-bis(3-bromopropyl)-9′,9′-bis(2-methoxyethyl)-9*H*,9′*H*-[2,2′-bifluoren]-7-yl)phenyl-9*H*,9′*H*-[2,2′-bifluorene]-9,9-diyl)bis(*N*,*N*,*N*-trimethylpropan-1-aminium) bromide (C_{60}-2HMTPB) and [6,6]-phenyl-C_{61}-butyricacid-2-(4-(9′,9′-bis(3-bromopropyl)-9,9-bis(2-(2ethoxyethoxy)-ethyl)-9*H*, 9′*H*-[2,2′-bifluoren]-7-yl)phenyl-9*H*,9′*H*-[2,2′-bifluoren]-9-yl)-*N*,*N*,*N*-trimethylpropan-1-aminium (C_{60}-2EHTPB) were designed and synthesized successfully. Our group have reported a conjugated amphiphilic diblock fullerene derivatives named [6,6]-phenyl-C_{61}-butyricacid-4-(9,9,9′,9′-tetrakis(3-bromopropyl)-9*H*,9′*H*-[2,2′-

* Corresponding author.
E-mail address: tgl@hust.edu.cn (G. Tu).

https://doi.org/10.1016/j.cclet.2019.05.023
1001-8417/

bifluoren]-7-yl)-phenol-(*N,N,N*-trimethylpropan-1-aminium)-bromide (C_{60}-4TPB) and applied in inverted OSCs based on poly[[4,8-bis[(2-ethylhexyl)oxy]benzo[1,2-b:4,5-b']dithiophene-2,6-diyl][3-fluoro-2-[(2-ethylhexyl)-carbonyl]thieno[3,4-b]thiophenediyl]] (PTB7) [6,6]:-phenyl-C_{71}-butyric acid methyl ester ($PC_{71}BM$) blend [47]. The C_{60}-2HMTPB and C_{60}-2EHTPB had a great similar structure with C_{60}-4TPB, and the two new fullerene derivatives were all applied to modify ZnO. The polar groups in the side chains of C_{60}-2HMTPB was *N,N,N*-trimethylpropan-1-aminium bromide ($-C_6H_{15}BrN$) and methoxyethane ($-C_3H_7O$). While the fullerene derivatives C_{60}-2EHTPB had polar groups of $-C_6H_{15}BrN$ and 1,2-diethoxyethane ($-C_6H_{13}O_2$) on the side chains of fluorene block. The position of quaternary ammonium salt and ether chain in C_{60}-2HMTPB and C_{60}-2EHTPB was different. The inverted OSCs devices based on ZnO/fullerene derivatives electronic transport layer (ETL) with a blend of poly[4,8-bis(5-(2-ethylhexyl)thiophen-2-yl)benzo-[1,2-b;4,5-b']dithiophene-2,6-diyl-*alt*-(4-(2-ethylhexyl)-3-fluorothieno [3,4-b]-thiophene)-2-carboxylate-2-6-diyl)] (PTB7-Th): $PC_{71}BM$ blend were also prepared and tested. The device architecture for the inverted OSCs and chemical structure of the three conjugated amphiphilic fullerene derivatives were showed in Fig. 1. Owing to the functionalized hydrophilic groups, the three fullerene derivatives could form interfacial dipoles and lower the work function of ZnO, boosting the charge extraction and enhancing the power conversion efficiency (PCE) of OSCs devices. Notably, the solvent annealing of toluene was also introduced on fullerene derivatives, and a well-defined morphology of the self-assembled ZnO/fullerene derivatives layer was supported by X-ray diffraction (XRD) and contact angle of water measurements [11,48]. The work function of ZnO also had an obvious reduction caused by interfacial dipole that formed by hydrophilic block of conjugated fullerene derivatives, thus leading lowest unoccupied molecular orbital (LUMO) energy levels of −3.84 eV, −3.93 eV and −3.77 eV for ZnO/C_{60}-4TPB, ZnO/C_{60}-2HMTPB and ZnO/C_{60}-2EHTPB, respectively. The devices based on different ZnO/fullerene derivatives ETLs also got PCEs of 8.62%, 8.83% and 9.00% for C_{60}-4TPB, C_{60}-2HMTPB and C_{60}-2EHTPB, respectively. The enhancement of PCE for devices based on ZnO/fullerene derivatives ETLs should be ascribed to the simultaneous enhancement of short circuit current (*Jsc*), which was caused by a better interfacial contact between ZnO and active layer.

The synthetic scheme of C_{60}-4TPB, C_{60}-2HMTPB and C_{60}-2EHTPB was shown in Scheme 1, and the ^1H NMR spectra of products were shown in Figs. S1–S17 (Supporting information). The two new synthesized conjugated amphiphilic triblock fullerene derivatives were obtained from an esterification reaction between the carboxyl (—COOH) of hydrophobic fullerene block and the hydroxyl (—OH) of hydrophilic conjugated fluorene block, and they have similar conjugated structure with each other between the hydrophilic block. The conjugated amphiphilic triblock fullerene derivatives C_{60}-2EHTPB can be regarded as

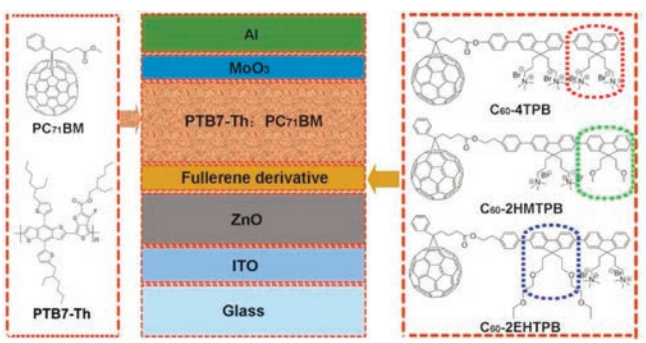

Fig. 1. Device architecture for the inverted organic solar cells and molecular structures of $PC_{71}BM$, PTB7-Th, C_{60}-4TPB, C_{60}-2HMTPB and C_{60}-2EHTPB.

hydrophilic-amphiphilic-hydrophobic triblock molecular, while C_{60}-2HMTPB can be classified in type of amphiphilic-hydrophilic-hydrophobic triblock molecular, in which fullerene is the hydrophobic block, the fluorene blocks with *N,N,N*-trimethylpropan-1-aminium bromide ($-C_6H_{16}BrN$) on side chains were the hydrophilic block, and the fluorene with ether chain on side chains was the amphiphilic block. The difference between the two triblock molecular was the location of amphiphilic block and hydrophilic block. The reported fullerene derivatives C_{60}-4TPB can be regarded as a conjugated amphiphilic diblock fullerene derivatives, which was also used to be a reference in this work. Thanks to the functionalized groups of amphiphilic and hydrophilic blocks, the three fullerene derivatives can be readily dissolved in polar solvents dimethyl sulfoxide (DMSO). The three-dimensional architecture of $PC_{61}BA$, 4TPB, 2HMTPB, 2EHTPB, C_{60}-4TPB, C_{60}-2HMTPB and C_{60}-2EHTPB were showed in Fig. S18 (Supporting information), and the benzene structure in hydrophilic conjugated fluorene block and fullerene structure formed the main conjugated chain of the two amphiphilic diblock fullerene derivatives.

The UV–vis absorption of $PC_{61}BA$, 4TPB, 2HMTPB, 2EHTPB, C_{60}-4TPB, C_{60}-2HMTPB and C_{60}-2EHTPB were displayed in Fig. S19 (Supporting information). For $PC_{61}BA$, the peaks of 330 nm and 435 nm were the characteristic absorption of $PC_{61}BA$. 2HMTPB and 2EHTPB all had an absorption peak at 345 nm, while 4TPB had absorption at 351 nm. The obvious absorption peaks was caused by the conjugated structure and the phenomenon of red shift between 2HMTPB and 4TPB may be caused by the various functional group on fluorene block. For the three fullerene derivatives, C_{60}-2HMTPB and C_{60}-2EHTPB had an obviously wide absorption peak from 315 nm to 380 nm, while the absorption peak of C_{60}-4TPB from 315 nm to 380 nm was weak. The author accounted that the wide absorption peak of the three fullerene derivatives was caused by the strong intra-molecule effect between hydrophobic fullerene block and hydrophilic conjugated fluorene block. Compared with $PC_{61}BA$, 4TPB, 2HMTPB and 2EHTPB, the UV–vis absorption was also an evidence to confirm the structure of C_{60}-4TPB, C_{60}-2HMTPB and C_{60}-2EHTPB.

In considering the amphipathic characteristics of the three fullerene derivatives, the toluene solvent annealing was introduced during the preparation of OSCs devices, and the XRD and water contact angle measurement were taken to test the self-assembly of fullerene derivatives. For the XRD measurement, it was conducted to investigate the crystallinity and molecular orientation of ZnO and ZnO/fullerene derivative films [49–51]. The samples of ITO/ZnO/fullerene derivatives without and with toluene treatment were named thermal annealing (TA) and solvent annealing (SA) samples, respectively. It is can be found in Fig. S20 (Supporting information), both the TA and SA ZnO films had exhibited weak diffraction peaks locates at 30 degree appearing in the XRD spectra, which indicated that the treatment of toluene had an ignored effect on the molecular distribution of ZnO. However, for the ZnO/fullerene derivatives films, both the three films exhibited obvious different diffraction peaks between TA and SA samples, especially the ZnO/C_{60}-2HMTPB film. Before the treatment of toluene, the diffraction peaks located at 30 degree of the three ZnO/fullerene derivatives films were weak. This indicated that the three fullerene derivatives were disorder on the surface of ZnO. While for the SA samples, the diffraction peaks of ZnO/fullerene derivatives films increased obviously. The enhancement of diffraction peaks should be ascribed to the increased order of the fullerene derivatives, which was caused by the rigidity of the fullerene structure (PCBM) and fluorene conjugate structure under the treatment of toluene. Under the treatment of toluene, the three fullerene derivatives could have an obvious self-assembly on ZnO, and the hydrophilic block and hydrophobic block in the three amphiphilic triblock fullerene derivatives can regulate the stacking

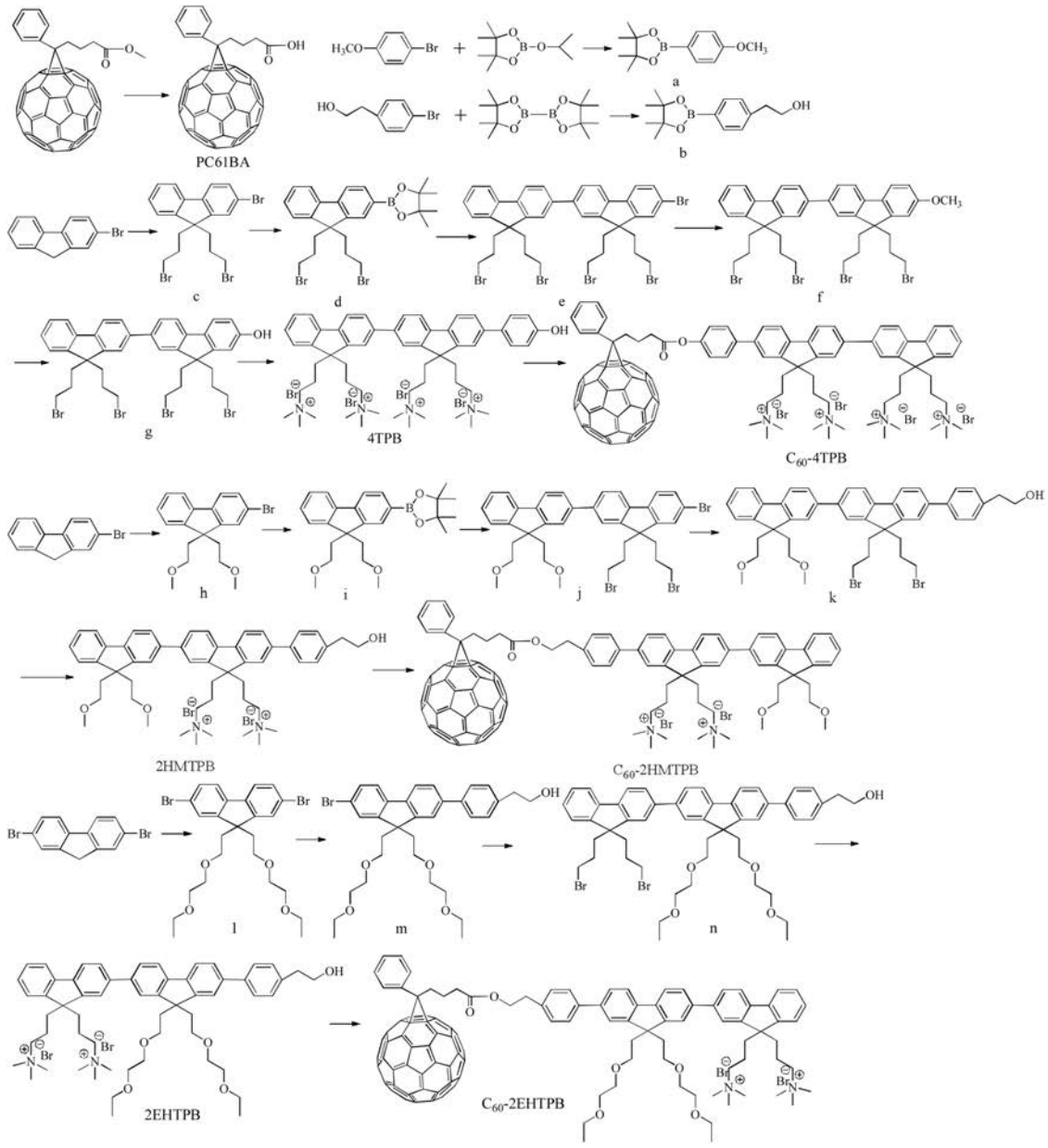

Scheme 1. Synthetic scheme of C_{60}-4TPB, C_{60}-2HMTPB and C_{60}-2EHTPB.

of molecules. The difference of diffraction peaks in XRD spectrum between TA and SA ITO/ZnO/fullerene derivatives (C_{60}-4TPB, C_{60}-2HMTPB and C_{60}-2EHTPB) samples supported that the treatment of toluene could cause an obvious self-organization of fullerene derivatives on ZnO layer. By introducing the solvent treatment is an effective way to modulate the molecular stacking orientation, and the increased crystallization performance indicated the high degree of molecular ordering was beneficial to the charge transport and resulted in less charge recombination, as evidenced by the improved J_{sc}. It is supposed that the better crystallinity and stacking orientation of ETL layers should be the main reason for the high PCEs of devices based on ZnO/fullerene derivatives ETLs. The photographs of water droplets on the surfaces of ITO/ZnO and ITO/ZnO/fullerene derivatives samples were showed in Fig. S21 (Supporting information). In general, the surface energy and wetting coefficient had close relationship with the water contact angle measurement. The contact angle is an important factor of wetting ability. The smaller the water contact angle on the surface of sample, the better the wetting coefficient between the water and films and the higher the surface energy will be. On the contrary, if the sample had a lower surface energy, then the water droplets cannot be well wetted on the surface of films, and the water contact angle is larger. The photographs of water droplets on the surfaces of ITO/ZnO/fullerene derivatives films indicated the distribution orientation of hydrophilic and hydrophobic blocks in the three amphipathic molecules. There is no difference between the water contact angle on the surface of TA and SA ITO/ZnO samples, which were all 48 degree. This result demonstrated that the treatment of toluene for 24 h had scarcely effect on ZnO layer. When spin-coated on ZnO, the hydrophilic block of conjugated amphiphilic triblock fullerene derivatives tend to the ZnO surface, leaving the fullerene cage facing block toward the opposite direction. The photographs of water droplets were dependent on the wetting properties between water and the polarity of outermost layer of the films. Based on the diversity polarity of bare ZnO and fullerene block, the variety shape of water

droplets were formed on the surface of films. The water contact angles were 72.5 and 68 degrees for C_{60}-2HMTPB and C_{60}-2EHTPB on TA films, respectively. While the water contact angle were 79 and 80 degrees on SA ITO/ZnO/C_{60}-2HMTPB and SA ITO/ZnO/C_{60}-2EHTPB films. For conjugated amphiphilic diblock fullerene derivatives C_{60}-4TPB, the water contact angle were 75 degree and 79.5 degree for TA and SA films respectively, thus was also match with the more fullerene toward the opposite direction of ZnO caused by the self-organizing. The water contact angle of SA samples all had an obvious enhancement compared with the corresponding TA samples, which can attribute that more hydrophobic fullerene cage at the top surface after the treatment of toluene, indicating the self-organization of fullerene derivatives. The TA ITO/ZnO/C_{60}-2EHTPB sample had the lowest water contact angle on the surface, which indicated that the C_{60}-2EHTPB film on ZnO had the best surface energy and the highest wetting coefficient. The results of XRD spectrum and water contact angle between TA and SA ITO/ZnO/fullerene derivatives samples all demonstrated that the treatment of toluene could cause a self-organization of fullerene derivatives on ZnO, and the self-assembly of the three fullerene derivatives were also match with their amphiphilic characteristic.

Surface topography atomic force microscope (AFM) images measurements were performed to confirm the surface morphology of ITO/ZnO/fullerene derivatives samples, as showed in Fig. 2. For ITO/ZnO, it was distributed on ITO substrate uniformity and the root mean square (RMS) was 2.67 nm with a surface height difference was around 10 nm (Fig. 2a). The smooth surface of films demonstrated that ZnO had well wetting properties with ITO, which can guarantee an appropriate characteristic between ZnO and ITO. The surface of ITO/ZnO/C_{60}-4TPB showed a rough RMS of

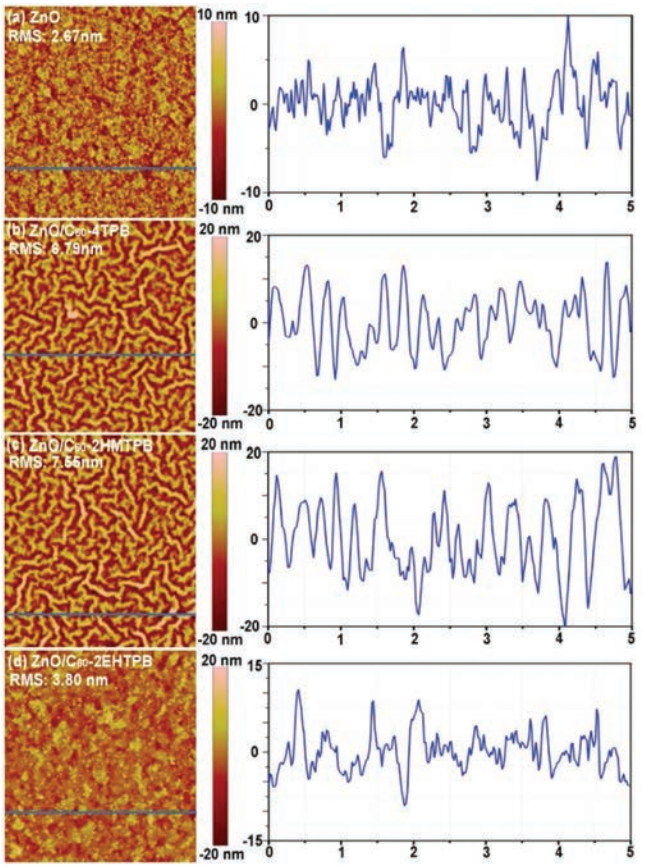

Fig. 2. Surface topography AFM images (5 um × 5 um) of samples: (a) ITP/ZnO, (b) ITO/ZnO/C_{60}-4TPB, (c) ITO/ZnO/C_{60}-2HMTPB, (d) ITO/ZnO/C_{60}-2EHTPB.

6.79 nm and the surface height difference was about 20 nm. The rough surface of film was due to the incompatibility of wetting properties between the hydrophilic block of C_{60}-4TPB and ZnO layer. The blocks of conjugated fluorene with hydrophilic groups of bare quaternary ammonium salt (—$C_6H_{15}BrN$) in C_{60}-4TPB have not showed a well wetting properties with ZnO, thus leading more aggregation formed on surface of ZnO and more rough surface (Fig. 2b). The RMS of ITO/ZnO/C_{60}-2HMTPB was 7.55 nm and the fullerene derivative C_{60}-2HMTPB was also formed in aggregation with sharp shape on ZnO (Fig. 2c). The surface height difference was around 25 nm, which was much rougher than ZnO. The results of RMS and surface height difference demonstrated that C_{60}-2HMTPB also had incompatibility wettability with ZnO, which lead much aggregation of on ZnO. However, the ITO/ZnO/C_{60}-2EHTPB sample had almost no aggregation on surface, with RMS of 3.80 nm and surface height difference of 10 nm (Fig. 2d). The smooth surface of films showed well wetting properties between ZnO and fullerene derivatives C_{60}-2EHTPB. The results of surface topography demonstrated that the molecule three different fullerene derivatives had different wetting properties with ZnO, and thus also lead various surface topography on ZnO. The results of AFM image was also match with photographs of water droplets formed on ITO/ZnO and ITO/ZnO/fullerene derivatives.

The X-ray photoelectron spectroscopy (XPS) spectra of ITO/ZnO and ITO/ZnO/fullerene derivatives samples were showed in Fig. 3. It was expected that C_{60}-4TPB, C_{60}-2HMTPB and C_{60}-2EHTPB layer were formed on top of the ZnO by reaction between the hydrophilic groups of the fullerene derivatives with the ZnO surface. The O 1s XPS spectrum of ITO/ZnO exhibits two typical peaks, located at about 529.8 eV and 531.0 eV (Fig. 3a). The peak at lower binding energy corresponds to the Zn—O bonds. The other peak at higher binding energy is ascribed to oxygen atoms from hydroxyl oxygen. Besides the two peaks from ZnO, there were additional peaks in O 1s XPS spectrum of 532.5 eV for C_{60}-4TPB, 531.7 eV for C_{60}-2HMTPB and 531.8 eV for C_{60}-2HMTPB respectively, which was caused by carboxyl groups (COOR). Fig. 3b presented the C 1s XPS spectra of ITO/ZnO, ITO/ZnO/C_{60}-4TPB, ITO/ZnO/C_{60}-2HMTPB and ITO/ZnO/C_{60}-2EHTPB samples. It is found that all the samples have two peaks ~284.5 eV (R-C_3H_7) and ~288.6 eV (COOR), which is assigned to the C atoms of carbonyl groups. The atomic concentrations of carbon, oxygen and zinc in all the samples based on the O 1s, C 1s and Zn 2p XPS spectra are summarized in Fig. 3c. When the three fullerene derivatives were spin coated on ZnO, the hydrophilic groups tend to the ZnO surface, leaving the hydrophobic and carbon-rich fullerene cage facing toward the opposite direction. In that case, more carbon and less oxygen were detected. With ZnO layer covered by fullerene derivatives layer, the bare ZnO became less, thus also leading a decrease atomic concentrations of zinc. The XPS spectra of all atomics were shown in Fig. S22 (Supporting information). For ITO/ZnO sample, the elements of Zn, O, Sn, In and C were all measured. While the three ITO/ZnO/fullerene derivatives samples all had an obvious increasing peaks of C, which attributed to fullerene block. The additional element peaks of N were the feature element of the three moleculers, which was also different with bare ZnO. The XPS spectra indicated that C_{60}-4TPB, C_{60}-2HMTPB and C_{60}-2EHTPB were present on the ZnO surface successfully.

The Ultraviolet photo-electron spectroscopy (UPS), UV–vis absorption spectra and energy level diagrams of ITO/ZnO and ito/ZnO/fullerene derivatives samples were showed in Fig. S23 (Supporting information), and the energy levels of ZnO and ZnO/fullerene derivatives films were summarized in Table S1 (Supporting information). The polar hydrophilic groups in the fullerene derivatives C_{60}-4TPB, C_{60}-2HMTPB and C_{60}-2EHTPB preferred to form an aligned dipole moment at the metal electrode/organic active layer interface, which can modify the work function of the

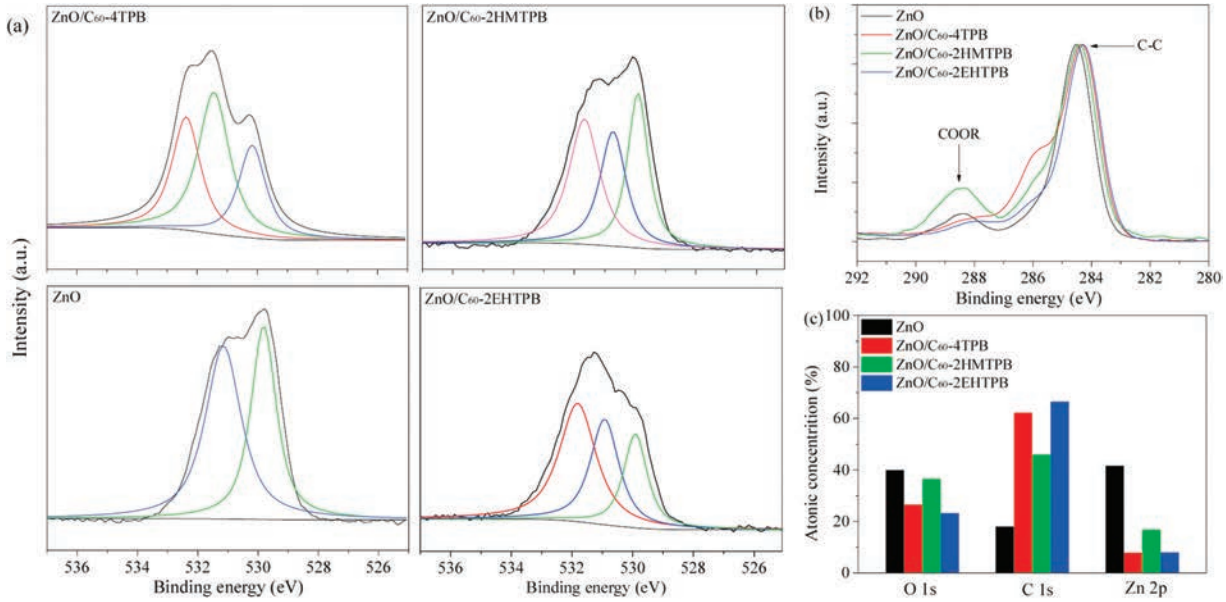

Fig. 3. XPS spectra of ITO/ZnO, ITO/ZnO/C_{60}-4TPB, ITO/ZnO/C_{60}-2HMTPB and ITO/ZnO/C_{60}-2EHTPB samples: (a) O 1s, (b) C 1s spectra and (c) atomic concentrations of carbon, oxygen and zinc.

electrode. UPS spectra in Fig. S23a (Supporting information) is performed to explore the effects of the fullerene derivatives on the energy levels of ZnO. The highest occupied molecular orbital (HOMO) level energies are defined according to the Eq. (1) (where hν was the incident photon energy of 21.2 eV, and $E_{\text{cut off}}$ was gained from high binding energy cutoff of a spectrum [52], $E_{\text{onset}}^{\text{HOMO}}$ was delivered from the right panel).

$$E_{\text{HOMO}} = \text{h}\nu - \left(E_{\text{onset}}^{\text{HOMO}} - E_{\text{cut off}}\right) \quad (1)$$

The HOMO energies of ITO/ZnO, ITO/ZnO/C_{60}-4TPB, ITO/ZnO/C_{60}-2HMTPB and ITO/ZnO/C_{60}-2EHTPB were −7.78 eV, −7.13 eV, −6.98 eV and −6.79 eV, respectively. The band gap for ITO/ZnO/C_{60}-4TPB, ITO/ZnO/C_{60}-2HMTPB and ITO/ZnO/C_{60}-2EHTPB were obtained from UV–vis absorption spectrum, which were 3.29 eV, 3.05 eV and 3.02 eV, as showed in Fig. S23b (Supporting information). When the three fullerene derivatives as modification layer on ZnO, the lowest unoccupied molecular orbital (LUMO) energy levels were −3.84 eV, −3.93 eV and 3.77 eV for ITO/ZnO/C_{60}-4TPB, ITO/ZnO/C_{60}-2HMTPB and ITO/ZnO/C_{60}-2EHTPB respectively, compared to −4.58 eV of ITO/ZnO. In addition, the results of UPS demonstrated that a strong interfacial interaction and interfacial dipole have been formed in the interface of ZnO and the three fullerene derivatives, which can decrease the work function of the ZnO, which can also improve the interfacial contact between ZnO and active layer. The interfacial dipoles originate from the dipole moments of fullerene derivatives itself and the interfacial interaction between fullerene derivatives and ZnO. This improved interfacial contact is beneficial for charge separation and transport [53]. The transmittance spectra of ZnO and ZnO/fullerene derivatives films were showed in Fig. S23c (Supporting information). Both ZnO and ZnO/fullerene derivatives films showed high transmittance in the range of 400–800 nm. At a wavelength of approximately 400 nm, all the ZnO/fullerene derivatives film showed lower transmittance than the ZnO film, which can be explained by the absorption of the three fullerene derivatives. The energy level diagrams of ZnO and ZnO/fullerene derivatives films was showed in Fig. S23d (Supporting information), C_{60}-2EHTPB was the best choice to modify ZnO among the three fullerene derivatives.

In order to study the performance of OSCs after introducing the three fullerene derivatives layer, the inverted OSCs based on PTB7-Th:$PC_{71}BM$ system with basic structure of ITO/ZnO/fullerene derivatives/active layer/MoO_3/Al was fabricated, and the parameters of OSCs devices were summarized in Table 1. The devices based on ZnO modified by the three fullerene derivatives all showed enhancement Jsc than bare ZnO. For ZnO modified by C_{60}-4TPB, the device exhibited PCE of 8.62% with V_{oc} of 0.79 V, J_{sc} of 17.00 mA/cm^2 and FF of 64.55%. The devices based on ZnO/C_{60}-2HMTPB ETL also exhibited PCE of 9.24% with V_{oc} of 0.79 V, J_{sc} of 18.09 mA/cm^2 and FF of 65.18%. The devices with ZnO/C_{60}-2EHTPB ETL exhibited PCE of 9.00% with V_{oc} of 0.79 V, J_{sc} of 18.08 mA/cm^2 and FF of 62.78%. Meanwhile, the device based on ZnO reached PCE of 8.13%, with V_{oc} of 0.78 V, J_{sc} of 16.71 mA/cm^2 and FF of 62.47%. The notable efficiencies based on the ZnO/fullerene derivatives ETL should be ascribed to the simultaneous enhancement of Jsc, as showed in Fig. 4a. The J_{sc} values were enhanced from 16.71 mA/cm^2 to 17.00 mA/cm^2, 17.50 mA/cm^2 and 18.08 mA/cm^2 for C_{60}-4TPB, C_{60}-2HMTPB and C_{60}-2EHTPB based devices, respectively. The dark current curves were shown in Fig. 4b, in which it was obvious that the dark current densities of the ZnO/fullerene derivatives interfacial layers under reverse bias were smaller than that of the bare ZnO interfacial layer, which meant that the leakage current at negative voltages was greatly inhibited by the amphiphilic diblock fullerene derivatives. The dark current curve also demonstrateed that the favorable

Table 1
Device parameters of the inverted OSCs devices with the structure of ITO/ETLs/PTB7-Th:$PC_{71}BM$/MoO_3/Al based on different ETLs under the illumination of AM 1.5 G, illumination at 100 mW/cm^2.

ETLs	V_{oc} (V)	J_{sc} (mA/cm^2)	FF (%)	PCE (%)
ZnO	0.78 ± 0.005	16.71 ± 0.02	62.47 ± 0.08	8.13 ± 0.11
ZnO/C_{60}-4TPB	0.79 ± 0.008	17.00 ± 0.08	64.55 ± 0.20	8.62 ± 0.10
ZnO/C_{60}-2HMTPB	0.79 ± 0.006	17.50 ± 0.06	63.70 ± 0.25	8.83 ± 0.13
ZnO/C_{60}-2EHTPB	0.79 ± 0.007	18.08 ± 0.10	62.78 ± 0.15	9.00 ± 0.10

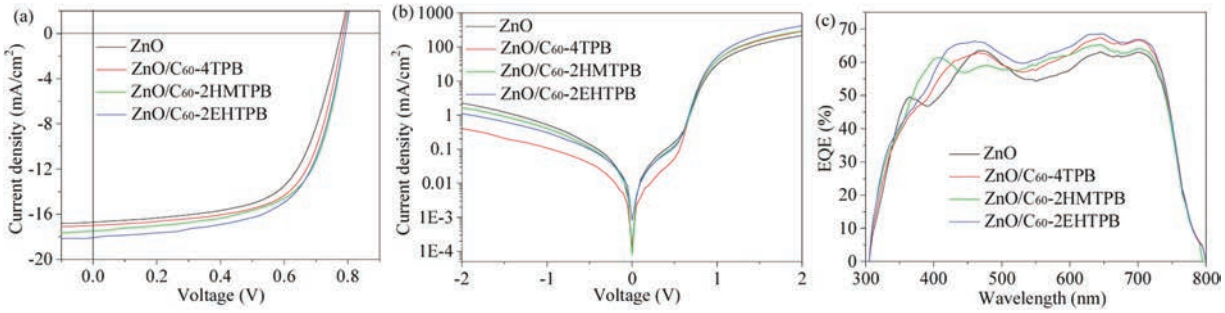

Fig. 4. Photovoltaic performance curves of devices: (a) J–V characteristics, (b) dark current and (c) EQE curves.

interfacial dipole caused by the fullerene derivatives reduces the leakage current and enhances the charge injection efficiency. The EQE curve was also represented to further verify the device performance. As presented in Fig. 4c, the device based on ZnO/fullerene derivatives all showed better EQE than bare ZnO from 300 to 800 nm, which is completely consistent with the results obtained from the J–V characteristics. The J_{sc} values calculated from the EQE curves under the standard solar spectrum (AM 1.5 G) were 14.32 mA/cm^2 for bare ZnO, 14.76 mA/cm^2 for ZnO/C_{60}-4TPB, 14.78 mA/cm^2 for ZnO/C_{60}-2HMTPB and 15.01 mA/cm^2 for ZnO/C_{60}-2EHTPB, respectively. The enhancement of *Jsc* and PCEs were in good agreement with the energy level and surface topography of bare ZnO and ZnO/fullerene derivatives films. Due to the aligned dipole moment at the ZnO/active layer interface, the interfacial contact is beneficial for enhanced charge transport and suppressed interfacial recombination. It was observed that the deposition of the three fullerene derivatives on ZnO layer could efficiently decrease the dark current, and forms better interfacial contact between ZnO and the active layer.

In conclusion, two conjugated amphiphilic triblock fullerene derivatives C_{60}-2HMTPB and C_{60}-2EHTPB were synthesized, which had great similar structure with our reported conjugated amphiphilic diblock fullerene derivatives C_{60}-4TPB, and the three of them were also used to modify ZnO. Both the three fullerene derivatives could exhibit an obvious self-assemble on ZnO surface with a treatment of toluene, which can be supported by XRD and water contact angle measurement. When applied to modify the ZnO layer, the three fullerene derivatives can decrease the work function effectively by the interfacial dipole formed between ZnO and hydrophilic groups of molecules. Due to variety wetting properties with ZnO, the three molecules also showed different surface topographies on ZnO. When applied in the inverted OSCs based on PTB7-Th: $PC_{71}BM$ system, the devices also got PCEs of 8.62%, 8.83% and 9.00% for C_{60}-4TPB, C_{60}-2HMTPB and C_{60}-2EHTPB, compared with 8.13% of bare ZnO. The performances of modified devices were also well matched with the results of the UPS measurement. Considering the synthesis procedures, wetting properties and surface topographies on ZnO, parameters of OSCs devices, the conjugated amphiphilic triblock fullerene derivatives C_{60}-2EHTPB was the best choice to act as the interface material for modifying ZnO.

Acknowledgments

This work was financially supported by the National Key R&D Program of China (No. 2018YFA0209200), the National Natural Science Foundation of China (No. 21574049). The authors also thank the Analytical and Testing Center of Huazhong University of Science and Technology (HUST) for allowing us to use their facilities.

Appendix A. Supplementary data

Supplementary material related to this article can be found, in the online version, at doi:https://doi.org/10.1016/j.cclet.2019.05.023.

References

[1] L. Verheyen, B. Timmermans, G. Koeckelberghs, et al., Macromolecules 51 (2018) 6421–6429.
[2] M. Nasiri, D. Saxon, T. Reineke, et al., Macromolecules 51 (2018) 2456–2465.
[3] D. Ndaya, R. Bosire, L. Mahajan, et al., Polym. Chem. 9 (2018) 1404–1411.
[4] Y. Qi, B. Li, Y. Wang, et al., Polym. Chem. 8 (2017) 6964–6971.
[5] A. Ding, G. Lu, H. Guo, et al., Polym. Chem. 8 (2017) 7537–7545.
[6] Q. Xu, Y. Zhang, X. Li, et al., Polym. Chem. 9 (2018) 4908–4916.
[7] D. Lye, Y. Xia, M. Wong, et al., Macromolecules 50 (2017) 4244–4255.
[8] G. Zaldivar, M. Samad, M. Conda-Sheridan, et al., Soft Matter 14 (2018) 3171–3181.
[9] J. Palacios, A. Tercjak, G. Liu, et al., Macromolecules 50 (2017) 7268–7281.
[10] P. Zhou, Y. Liu, L. Niu, et al., Polym. Chem. 6 (2015) 2934–2944.
[11] W. Deng, K. Gao, J. Yan, et al., ACS Appl. Mater. Interfaces 10 (2018) 8141–8147.
[12] Y. Shin, C. Song, W. Lee, et al., Macromol. Rapid Commun. 38 (2017) 1700016.
[13] C. Jangu, J. Wang, D. Wang, et al., J. Mater. Chem. C 3 (2015) 3891–3901.
[14] J. Li, J. Liu, G. Tu, Solar Energy 181 (2019) 405–413.
[15] D. Zhou, S. Xiong, L. Chen, et al., Chem. Commun. 54 (2018) 563–566.
[16] Y. Yin, Y. Zhang, L. Zhao, et al., Macromol. Rapid Commun. 39 (2018) e1700697.
[17] M. Neophytou, D. Bryant, S. Lopatin, et al., Macromol. Rapid Commun. 39 (2018) e1700820.
[18] X. Li, S. Liu, K. Fan, et al., Adv. Energy Mater. 8 (2018) 1800101.
[19] Z. Jiang, H. Li, Z. Wang, et al., Macromol. Rapid Commun. 39 (2018) e1700872.
[20] H. Han, J. Seo, M. Song, et al., J. Mater. Chem. A 6 (2018) 7480–7487.
[21] X. Cai, T. Yua, X. Liu, et al., ACS Appl. Mater. Interfaces 9 (2017) 36082–36089.
[22] Y. Cheng, F. Cao, W. Lin, et al., Chem. Mater. 23 (2011) 1512–1518.
[23] M. Mahmud, N. Elumalai, M. Upama, et al., Nanoscale 10 (2018) 773–790.
[24] F. Wang, Y. Zhou, X. Pan, et al., Phys. Chem. Chem. Phys. 20 (2018) 6959–6969.
[25] Y. Tan, L. Chen, F. Wu, et al., Macromolecules 51 (2018) 8197–8204.
[26] J. Cao, B. Wu, R. Chen, et al., Adv. Mater. 30 (2018) 1705596.
[27] Y. Cui, H. Yao, B. Gao, et al., J. Am. Chem. Soc. 139 (2017) 7302–7309.
[28] S. Lu, H. Lin, S. Zhang, et al., Adv. Energy Mater. 7 (2017) 1701164.
[29] Y. Chao, Y. Huang, J. Chang, et al., J. Mater. Chem. A 3 (2015) 20382–20388.
[30] X. Zeng, J. Zhu, L. Yang, et al., J. Electron. Chem. 838 (2019) 94–100.
[31] Z. Zhang, X. Zhu, Chem. Mater. 5 (2018) 182–189.
[32] N. Tummala, S. Aziz, V. Coropceanu, et al., J. Mater. Chem. C 6 (2018) 3642–3650.
[33] S. Nam, J. Seo, M. Song, et al., Org. Electron. 48 (2017) 61–67.
[34] I. Jeon, S. Zeljkovic, K. Kondo, et al., ACS Appl. Mater. Interfaces 8 (2016) 29866–29871.
[35] S. Liao, H. Jhuo, Y. Cheng, et al., J. Mater. Chem. A 3 (2015) 22599–22604.
[36] Z. Zhang, H. Li, B. Qi, et al., J. Mater. Chem. A 1 (2013) 9624.
[37] X. Han, Z. Li, Z. Ding, et al., Nano Res. 11 (2018) 4293–4301.
[38] Y. Wang, X. Li, L. Zhu, et al., Adv. Energy Mater. 7 (2017) 1701144.
[39] C. Sun, Z. Wu, H. Yip, et al., Adv. Energy Mater. 6 (2016) 1501534.
[40] J. Wang, K. Lin, K. Zhang, et al., Adv. Energy Mater. 6 (2016) 1502563.
[41] J. Liu, J. Li, X. Liu, et al., Macromol. Chem. Phys. (2019) 1800477.
[42] C. Cui, Y. Li, Y. Li, et al., Adv. Energy Mater. 7 (2017) 1601251.
[43] C. Duan, K. Zhang, C. Zhong, et al., Chem. Soc. Rev. 42 (2013) 9071–9104.
[44] L. Derue, O. Dautel, A. Tournebize, et al., Adv. Mater. 26 (2014) 5831–5838.
[45] J. Liu, J. Li, G. Tu, Front. Optoelectron. 11 (2019) 348–359.
[46] T. Nguyen, T. Lee, B. Gautam, et al., Adv. Funct. Mater. 27 (2017) 1702474.
[47] J. Liu, J. Li, X. Liu, et al., ACS Appl. Mater. Interfaces 10 (2018) 2649–2657.
[48] J. Liu, C. Gao, X. He, et al., ACS Appl. Mater. Interfaces 7 (2015) 24008–24015.
[49] S. Xie, J. Wang, R. Wang, et al., Chin. Chem. Lett. 30 (2019) 217–221.
[50] Z. Wen, X. Ma, X. Yang, et al., Chin. Chem. Lett. 30 (2019) 995–999.
[51] Y. Shi, C. Yang, H. Li, et al., Chin. Chem. Lett. 30 (2019) 906–910.
[52] J. Seo, R. Yang, J. Brzezinski, et al., Adv. Mater. 21 (2009) 1006–1011.
[53] J. Kong, I. Hwang, K. Lee, Adv. Mater. 26 (2014) 6275–6283.